IEEE Access
Multidisciplinary | Rapid Review | Open Access Journal

Received April 9, 2020, accepted April 22, 2020, date of publication April 28, 2020, date of current version May 14, 2020.

Digital Object Identifier 10.1109/ACCESS.2020.2990956

Three-Port Optical Phase-Shifters and Modulators With Ultra-High Modulation Efficiency, Positive RF-Linking Gain, and Low Residual Amplitude Modulation

RUI LIN CHAO[1,2], ZOHAUDDIN AHMAD[2], JYEHONG CHEN[1], YINCHIEH LAI[1], AND JIN-WEI SHI[2], (Senior Member, IEEE)

[1]Department of Photonics, College of Electrical and Computer Engineering, National Chiao Tung University, Hsinchu 30010, Taiwan
[2]Department of Electrical Engineering, National Central University, Taoyuan City 32001, Taiwan

Corresponding author: Jin-Wei Shi (jwshi@ee.ncu.edu.tw)

This work was supported by the Ministry of Science and Technology in Taiwan under Grant MOST 106-2221-E-008 -063 -MY3 and Grant MOST 107-2218-E-009 -056 -

ABSTRACT A three-port optical phase-shifter and Mach-Zehnder modulator (MZM) based on PNP-type bipolar junction transistor (BJT) is demonstrated. Significant plasma (injected carrier) induced changes of the refractive index for the optical waveguide become possible with an extremely small driving-voltage and a compact device size during operation of this BJT between the saturation and forward active modes. Devices with a standard MZM structure and a small foot-print (0.5 mm) exhibit a moderate optical insertion loss (2 dB), extremely small V_π (0.18V) and P_π (0.21mW), fast rise/fall time (∼1ns), and a residue-amplitude-modulation (RAM) as small as 0.18 dB. Furthermore, thanks to the ultra-high modulation efficiency characteristic of our device, a +4.0 dB net RF-linking gain can be obtained under dynamic operation. Compared to 2-port (base-collector) forward bias operation, under three-port operation, the extra bias current from the base-emitter junction provides a lower V_π (0.18 vs. 0.22 V), a smaller RAM (0.18 vs. 0.6 dB), and a larger RF-linking gain (+4 vs. −3.2 dB). The superior performances of the three-port to two-port operations can be attributed to the additional forward bias B-E junction being able to provide more injected carriers to induce stronger plasma effects for optical phase-shifting.

INDEX TERMS Optical phase shifter, photonics integrated circuits, RF-linking gain, silicon photonics.

I. INTRODUCTION

Silicon photonics (SiPs) play a leading role in the development of technology ranging from radio frequency (RF) microwave photonics to sensing systems. For the application of microwave photonics, a net RF linking gain can greatly enhance the signal-to-noise (S/N) ratio in the communication channel. In order to attain a positive linking gain, a photodiode with a high output saturation current (power) [1] and a low-loss optical modulator with a small driving-voltage and the capability of handling high input optical power [2], is highly desired in the receiver and the transmitter side, respectively. However, the realization of a positive net RF linking gain is difficult on the SiP platform due to the fact that the required driving voltage for the π phase-shift at the reverse bias regime of Silicon based modulators is usually large (nearly ten volts) [3]–[5]. Increasing the p-type doping density in the active volume is one of the most effective ways to reduce the driving-voltage, but this leads to a significant optical insertion loss [3], [4]. On the other hand, with respect to the application of the sensing system, power-efficient and fast-switching optical phase shifters are essential to provide rapid beam steering speed [6]. High frame-rate image scanning is required for the operation of autonomous vehicles, in order to actively detect obstacles in front of them. On average, a scanning time of less than 6.1μs is necessary to rapidly react to these upcoming situations [7]. SiP based optical phase arrays (OPAs) have attracted a lot of attention for this purpose

The associate editor coordinating the review of this manuscript and approving it for publication was Muguang Wang.

due to their small footprint and the possibility of CMOS compatible optics-electronic integration. Thermo-optics resistive phase-shifters are popular because of their simple structure and small footprint [7]–[12], but device performance has been constrained by large power consumption (>12mW) and longer than μs scale switching/response time. On the other hand, the more conventional Mach-Zehnder interferometers (MZI) require high driving voltages (>6V; under reverse bias) for the π phase shift [4], [5], [13]. This impedes their application in optical phase arrays (OPA), which usually need to have hundreds of optical phase-shifters inside with a low-driving voltage for $>2\pi$ phase shifting [10]–[12]. Another approach has been to push the p-n junction of the MZI into the forward bias regime. This has been the most effective method to reduce the 2π driving-voltage but at the expense of lower modulation speed and higher power consumption [4], [5] as compared to MZIs operated under a reverse bias. Although the forward bias gain rolls off more rapidly with the increase of operating frequency, it offers a higher RF link gain improvement of more than 10 dB from nearly DC to 25 GHz [5]. Furthermore, forward bias operation is shown to result in a comparable spurious-free dynamic range [5]. Nevertheless, large (>2 dB) residual-amplitude-modulation (RAM), which leads to undesirable AM noise during phase modulation, usually happens in these forward-bias based p-n junction phase-shifters due to the free-carrier absorption loss induced by the high level injection carriers [4], [5].

In this work, we demonstrate three-port (PNP)-type bipolar junction transistor (BJT) based phase-shifters and MZMs fabricated on a standard commercial Si-photonic foundry platform. The measured output I_{EC}-V_{EC} characteristics of such devices operated in saturation mode are very similar to those of an ideal diode, which has a nearly zero turn-on voltage and an extremely small differential resistance. Furthermore, the additional base-emitter (p-n) junction in our three-port configuration can more efficiently inject or pull out the carriers inside the active waveguide, so that a phase shifter with a smaller footprint, smaller RAM, and lower driving-voltage than those of the two-port ones can thus be expected. With a short device length (0.5 mm) and an acceptable insertion loss (2 dB), our device exhibits excellent performance in terms of fast rise time ($t_R \approx$ 1ns), small driving-voltage and small power consumption for π phase-shift (P_π: 0.21 mW; V_π: 0.18 V), extremely small RAM (0.18 dB) [14], and a +4.0 dB net RF linking gain at an operating frequency of 100 MHz. Compared with our previous work [15], the doping profile is further optimized by greatly reducing the doping level in the p-type collector layer (from 3×10^{19} to 5×10^{17} cm^{-3}). By introducing this modification, we can attain a smaller optical insertion loss (2 vs. 6 dB) with the same value of V_π (~0.2 V). This is because that the plasma effect is induced in our structure by the injection of carriers from the B-E junction instead of the background doping. This ultra-high modulation efficiency and moderate optical insertion loss leads to a positive net RF linking gain (+4 dB) for the demonstrated switches during dynamic operation.

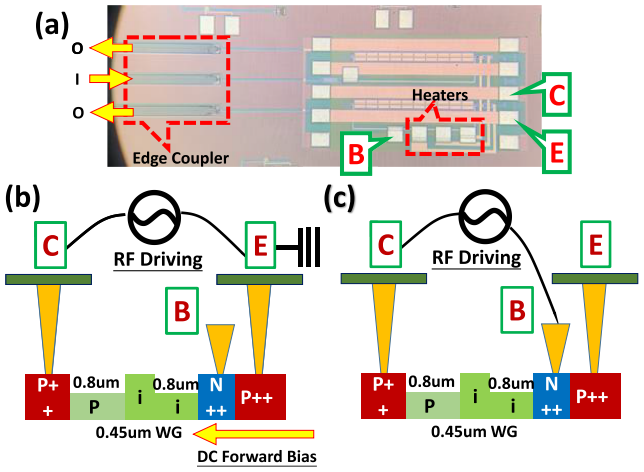

FIGURE 1. (a) Top view of the PNP BJT MZI fabricated by the IMEC foundry, Leuven, Belgium, Process Design Kit (PDK) 2.2.0. Conceptual cross-sectional plot of the PNP BJT MZI design under 3-port (b) and 2-port (c) operations. P^{++} (Emitter): 3×10^{20}, N^{++} (Base): 3×10^{20}, P (Collector): 5×10^{17}, P^{+}(sub-collector): 3×10^{19} cm^{-3}.

II. DEVICE STRUCTURE

Figure 1(a) shows a top view of the proposed device structure. Figures 1 (b) and (c) show a conceptual cross-sectional view of this device under 3-port (V_{EC}ac swing; V_{EB} dc bias) and 2-port (V_{CB} ac swing; emitter floating) operation, respectively. An optical waveguide (WG) 450 nm in width is sandwiched between the p (collector; C) and the n^{++}-type base (B), next to the neighboring p^{++} emitter (E) electrode in our pnp bipolar junction transistor (BJT) structure. Here, the actual doping levels for each layer are confidential information for the foundry. However, by performing capacitance-voltage (C-V) and transfer length method (TLM) measurements on the test keys, we can roughly estimate the doping level of each layer, as specified in the Figure 1 caption. The demonstrated phase-shifter, realized using the MZI structure, has a total device length of 500 μm. Figure 2 shows a conceptual diagram of the chip under test conditions. As can be seen, a multi-mode interference (MMI) power splitter provided by the IMEC process design kit (PDK 2.2.0) is adopted to split the incoming light into two optical arms. In the MZI, a directional coupler (50% for each port) is used to combine the modulated signal and send it to the output ports. As shown in Figure 1 (b), during high-speed operation, an AC modulation signal needs to be applied to the C and E pads for switching of the BJT device between the forward active and saturation regions to obtain significant changes in the output current (I_{CE}) and the plasma induced index change.

Compared with the traditional p-n junction two-port phase shifter, as shown in Figure 1(c), the extra p-n junction in our BJT structure can be used to more efficiently inject or pull out the carriers in the active volume, to obtain a phase shifter with a smaller footprint and lower driving-voltage. As shown in Figure 2, in our design, pads C and E can be probed by the high-speed ground/signal (GS) microwave probes to feed in the AC modulation signal for dynamic

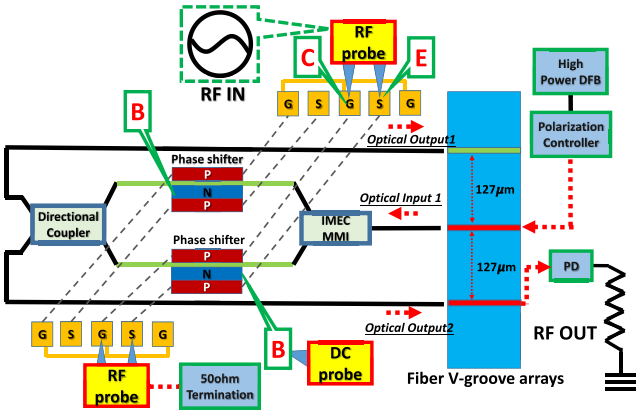

FIGURE 2. Conceptual diagram of the phase-shifter used in the test and measurement setup for determining the DC transfer curve and dynamic waveform.

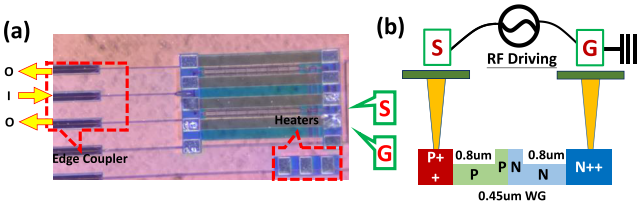

FIGURE 3. (a) Top view of the PN MZI fabricated by the IMEC foundry, Leuven, Belgium, Process Design Kit (PDK) 2.2.0. (b) The conceptual cross sectional plot of the PN MZI design. N: 5×10^{17} cm^{-3}.

operation. In addition, an external bias tee is connected to the GS microwave probe for application of the DC bias voltage to electrode C. For the BJT to operate in the desired modes, two DC probes are connected to electrodes B and E. As can be seen, the optical input signal is launched into the optical input port 1 (I1) and the waveguide is split into two channels to form the interferometer architecture by the IMEC PDK multimode interferometer (MMI). After individually passing through the junctions the channels are modulated by the RF slot line structure above them, with the optical power in the two channels combined together with different phase shifts by directional coupler. One of the two output ports (O1 and O2) is connected to a high-speed photo-receiver or optical power meter to measure the high-speed dynamic waveform and dc transfer curves, respectively. Here, we can define the RF linking gain as the ratio between the RF output signal from the PD module and the RF input signal used for driving our device (RF_{out}/RF_{in}), which are specified in Figure 2.

In order to have a good reference for comparison with the demonstrated BJT-type MZI, a traditional p-n junction based MZI is also realized on the same chip. Figures 3 (a) and (b) show a top view of the fabricated device and conceptual diagram of the reference PN junction MZI with the same active length (500 μm) as that of the PNP MZI.

III. MEASUREMENT RESULTS

Figure 4 shows the collector-emitter IV curves of our device given different values of V_{EB}bias voltage. During dynamic and static operation, our device operates in the saturation

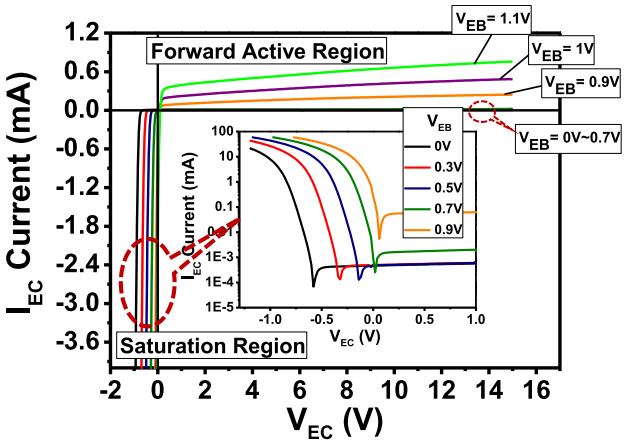

FIGURE 4. I_{EC}-V_{EC} curves measured under different applied V_{EB} voltages for our device. The inset shows an enlargement of the saturation region of the V_{EC}-I_{EC} curves.

regions (zone III), which indicates that both the V_{EB} and V_{CB} junctions are under forward bias. Clearly, tremendous increases in the output current (I_{EC}) versus V_{EC} bias are exhibited. The characteristics are similar to those indicated by the I-V curves of an ideal diode with a nearly zero turn-on voltage and a small differential resistance. The I-V characteristics can be understood as follows: Our BJT-type device is composed of two sets of PN-junctions (E-B and B-C junctions). A nearly zero turn on voltage (V_{EC}) at the C-E junction is observed when the E-B junction is under a 0.7 V forward bias ($V_{EB} = 0.7$). The turn-on current measured through the E-C junction is mainly generated from the forward bias E-B junction. On the other hand, when the E-B junction is zero biased ($V_{EB} = 0$), the turn-on voltage of the E-C junction increases to 0.7 V, which is equivalent to the application of a forward bias of 0.7 V to the C-B junction ($V_{CB} = 0.7$ V). Due to the large injected current and small voltage swing (0.1V), it is possible to produce a significant plasma induced change of the refractive index in the optical waveguide under an extremely small driving voltage, by switching the devices between saturation and forward active (zone I and III) modes.

Figure 5 (a) shows the measured DC transfer curves of the device under 2-port (V_{CB} swing) and 3-port (V_{EC} swing; $V_{EB} = 0$ V) operation. In the case of 2-port operation, the emitter terminal is left open and the bias voltage is applied to the B-C junction. It can be clearly seen that under 3-port operation the device can not only provide us with a smaller RAM (0.18 vs. 1.6 dB) but also a smaller V_π (0.18 vs. 0.22 V). The achieved RAM number (0.18 dB) is also much smaller than that reported for Si-photonic MZI under forward bias operation, where the RAM is usually as high as 2 dB [4], [5]. The smaller RAM of our device can be mainly attributed to the corresponding sweeping current ($I_{peak} - I_{valley}$) for V_π being as small as 2 mA. This number is smaller (2 vs. 4 mA) than that for the same device under 2-port operation (V_{CB} swing). Figure 5 (b) shows the transfer curves measured under different V_{EB} biases. The corresponding power consumption of each trace can be calculated as follows: the total power

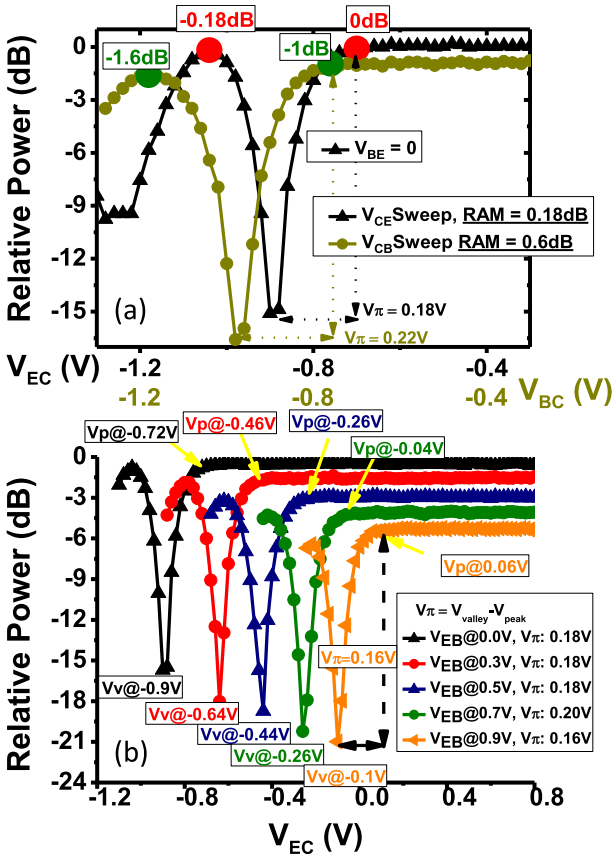

FIGURE 5. (a) Measured DC transfer curves under 2-port (V_{CB}) and 3-port (V_{EC}) swings. (b) Measured DC transfer curves under 3-port operation at different V_{EB} biases. V_V: Valley Voltage. V_P: Peak Voltage.

consumption is comprised of the dc bias at the B-E junction ($V_{EB} \times I_{EB}$) and the average power consumption of the ac driving signal into C-E junction ($(I_{peak} - I_{valley}) / 2 \times V_\pi$). We can clearly see that, even under a zero V_{EB} bias, we can still attain a small V_π (0.18 V) with an extremely small P_π (0.21 mW). The modulation speed and efficiency of the phase-shifter are both important issues for OPA applications as previously discussed. The dynamic measurement results for our device are discussed below.

Figures 6 (a), and (b) show the measured output waveforms of our MZI, as illustrated in Figure 2, under 2-port (V_{CB}) and 3-port (V_{EC}) operation, respectively. Here, the chosen V_{CB} and V_{EC} dc pre-bias points for dynamic operation are located at 0.92 and −0.05 V, respectively. These operation points simply correspond to the regions which have large slopes in their dc transfer curves, as shown in Figure 5.

We can clearly see that by applying an extra bias current onto the E-B junction for 3-port operation, we can greatly enhance the modulation efficiency and shorten the rise time (1.1 vs. 1.56 ns) of our MZI as compared to those obtained under 2-port operation and under the pretty close forward bias voltages ($V_{EB} \cong V_{CB} = 0.92$V). This reflects the truth that the 3-port operation can more effectively inject or pull-out the carriers inside active volume of waveguide than 2-port operation does. Furthermore, under a 100 mV

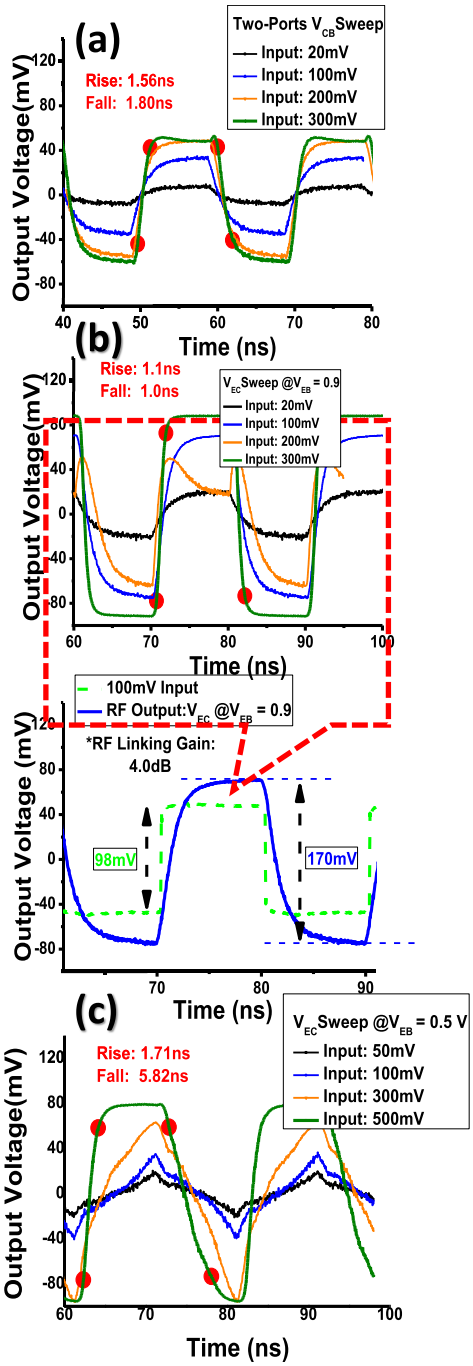

FIGURE 6. (a) Dynamic output waveforms from MZI switches for (a) two-port operation ($V_{CB} = 0.92$ V), (b) three-port operation ($V_{EC} = -0.05$ V; $V_{EB} = 0.9$V), and (c) three-port operation ($V_{EC} = -0.35$V; $V_{EB} = 0.5$V). The inset to (b) shows an enlargement of input/output waveforms with a 4.0 dB net RF-linking gain.

peak-to-peak driving voltage (V_{pp}), we have a net 4.0 dB RF power linking gain and a fast rise time (1.1 ns), as shown in the inset to Figure 6 (b). Nevertheless, in order to attain such a high modulation efficiency and fast response time, the required power consumption is around 9.1 mW due to the high V_{EB} forward bias voltage necessary (0.9 V). As shown in Figure 6 (c), by properly reducing the V_{EB} bias to 0.5V, we can retain the short rise time of 1.7 ns, with a larger

TABLE 1. Key performance metrics in previous state-of-the-art works.

Parameters	Direct Current Injection Adiabatic Waveguide	MMI Heater Inteferometer	Forward Bias PnN Junction	III-V SOI Heterogeneous Integration Carrier Depletion	PN Junction Carrier Depletion	PN Junction Carrier Depletion	PINP-Doped Type Phase Shifter (Three Ports)
Reference	7	9	4	14	16	17	**(This Work)**
Switching Time	2.4μs	2.16μs	Bandwidth: 0.1GHz	Rise Time: 0.2ns	Bandwidth: 21GHz	Rise Time: 60μs	**Rise Time: 1.1ns**
Power Consumption	12.7mW//π	28mW/π	0.22mW/π	(~nW)/π	-	0.71mW/π	**0.16mW/π**
Length	~10μm	~30 μm	250 μm	5000 μm	4000 μm	1250 μm	**500 μm**
Material	SOI	SOI	SOI	III-V + SOI	SOI	SOI	**SOI**
RAM	-	-	2.1dB	0.15dB	0dB~1dB	-	**0.18dB**
Vπ*L	-	(Vπ = 2.8V) 8.4V*μm	(Vπ = 0.11V) 25V*μm	(Vπ = 0.45V) 2250V*μm	(Vπ ~ 3.2V) 16000V*μm	(Vπ = 1.84V) 2300V*μm	**(Vπ = 0.18V) 90V*μm**
Insertion Loss	0.05dB/μm	0.037dB/μm	-	-	1.75dB/mm	8dB/mm	**0.004dB/μm**

output amplitude than that obtainable for 2-port operation (170 vs. 90 mV) while greatly reducing the dc power consumption to 0.9 mW. Table 1 shows the benchmark reported for phase-shifters on Si-photonic (SiP) platforms with state-of-the-art performance for OPA applications. Compared with the thermal-optics phase-shifter based on a standard SiP foundry, our device has a much faster response time, lower power consumption, and comparable insertion loss with an extremely small RAM, which satisfies the requirement for practical OPA applications. Here, the insertion loss (~2 dB for a length of 500 μm) is extracted by comparing devices with the same kind of structure but different active lengths. Compared to [15], we achieve a smaller optical insertion loss (2 vs. 6 dB) in this new structure, because of the reduction in the doping level in the p-type collector layer (3×10^{19} to 5×10^{17} cm^{-3}, as specified in Figure 1). which can effectively reduce the free-hole absorption loss. In addition, the reduction in the collector layer doping level has no significant influence on the driving-voltage performance (V_π: ~0.2 V), which is mainly determined by the amount of free carriers injected from the B-E junction rather than the background doping. Such ultra-high modulation efficiency and moderate optical insertion loss leads to a positive net RF linking gain (+4 dB) during dynamic operation of this novel device.

Figure 7 (a) shows the E-O responses of the PNP measured under 2- and 3-port operation and for the reference PN MZIs. It can be clearly seen that the PN MZI exhibits a much wider 3-dB E-O bandwidth (>20 GHz vs. ~1 GHz) than that of the PNP device. Nevertheless, the PNP devices have a much larger RF linking gain, which can be attributed to their extremely small V_π driving voltage (<0.2 V), with an operating frequency of less than 12 GHz. When the operating frequency becomes higher, the PN reference show a larger RF response due to the serious high-frequency roll-off of the PNP traces. This result indicates that the forward bias operation of Si MZI can benefit the narrow band analog RF linking when the frequency of the carrier signal is less than 12 GHz in our chip.

As illustrated in Figure 6, the net RF linking gain happens when the repetition rate of electrical pulses for MZI driving is low, tens of MHz. We thus narrow down the frequency span for E-O response measurement to study in detail the low-frequency behaviors of our devices. Figure 7 (b) shows the

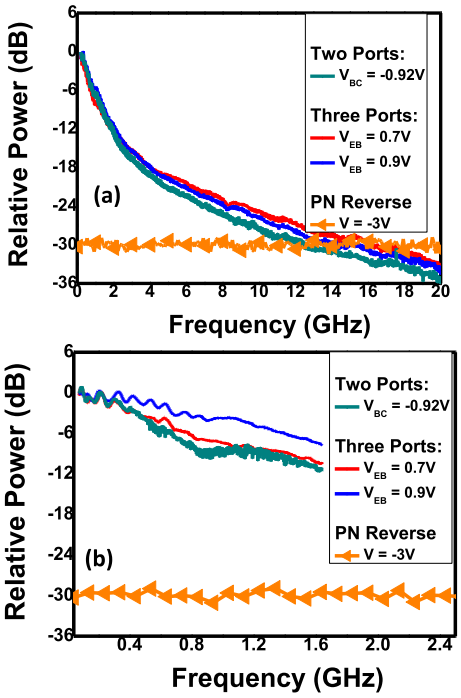

FIGURE 7. Measured E-O responses of PNP and reference PN MZIs obtained under different operation modes (2- and 3-ports), different operation voltages, and different measurement window spans (a) (dc to 20 GHz) and (b) dc to 2.5 GHz.

E-O responses measured under the same operation conditions as those shown in Figure 7 (a), but at a lower frequency band (40 MHz to 2.4 GHz). We can clearly see that for our device, the highest linking gain and widest E-O bandwidth among all the forward-bias operation conditions are provided under 3-port operation with a forward bias current through the B-E junction (V_{EB} = 0.9 V). This result is consistent with the time domain measurement results as discussed in Figure 6, where the rise time under three-port operation with a high V_{EB} forward bias (0.9 V) is faster (1.1 ns) than under a low V_{EB} (0.5 V; 1.71 ns) bias and two-port operation (1.56 ns).

IV. CONCLUSION

In this paper, we demonstrate a novel PNP bipolar junction transistor based optical phase-shifter fabricated on a Si-photonic foundry platform. With a small footprint (0.5 mm in length), such a device operated at saturation mode exhibits a small P_π/V_π (0.21 mW/0.18V), a reasonable insertion loss (2 dB), a small RAM (0.18 dB), and fast switching speed (t_R =~1.7 ns with 0.9 mW power consumption). A +4.0 dB net RF linking gain can also be achieved by increasing the bias current (voltage) on the B-E junction. These results show good potential of this device for the development of large scale PIC based optical scanners.

REFERENCES

[1] Z. Yang, Q. Yu, J. Zang, J. C. Campbell, and A. Beling, "Phase-modulated analog photonic link with a high-power high-linearity photodiode," *J. Lightw. Technol.*, vol. 36, no. 18, pp. 3805–3814, Sep. 15, 2018.

[2] W. K. Burns, M. M. Howerton, and R. P. Moeller, "Broad-band unamplified optical link with RF gain using a LiNbO3 modulator," *IEEE Photon. Technol. Lett.*, vol. 11, no. 12, pp. 1656–1658, Dec. 1999.
[3] R. Soref and B. Bennett, "Electrooptical effects in silicon," *IEEE J. Quantum Electron.*, vol. QE-23, no. 1, pp. 123–129, Jan. 1987.
[4] S. J. Spector, C. M. Sorace, M. W. Geis, M. E. Grein, J. U. Yoon, T. M. Lyszczarz, E. P. Ippen, F. X. Kärtner, "Operation and optimization of silicon-diode-based optical modulators," *IEEE J. Sel. Topics Quantum Electron.*, vol. 16, no. 1, pp. 165–172, Jan./Feb. 2010.
[5] R. L. Chao, J. W. Shi, A. Jain, T. Hirokawa, A. S. Khope, C. Schow, J. E. Bowers, R. Helkey, and J. F. Buckwalter, "Forward bias operation of silicon photonic Mach–Zehnder modulators for RF applications," *Opt. Express*, vol. 25, no. 19, pp. 23181–23190, Sep. 2017.
[6] J.-W. Shi, J.-I. Guo, M. Kagami, P. Suni, and O. Ziemann, "Photonic technologies for autonomous cars: Feature introduction," *Opt. Express*, vol. 27, no. 5, pp. 7627–7628, Feb. 2019.
[7] M. Mendez-Astudillo, M. Okamoto, Y. Ito, and T. Kita, "Compact thermo-optic MZI switch in silicon-on-insulator using direct carrier injection," *Opt. Express*, vol. 27, no. 2, pp. 899–906, Jan. 2019.
[8] M. W. Geis, S. J. Spector, R. C. Williamson, and T. M. Lyszczarz, "Sub-microsecond submilliwatt silicon-on-insulator thermooptic switch," *IEEE Photon. Technol. Lett.*, vol. 16, no. 11, pp. 2514–2516, Nov. 2004.
[9] M. R. Watts, J. Sun, C. DeRose, D. C. Trotter, R. W. Young, and G. N. Nielson, "Adiabatic thermo-optic Mach–Zehnder switch," *Opt. Lett.*, vol. 38, no. 5, pp. 733–735, Feb. 2013.
[10] J. Sun, E. Timurdogan, A. Yaacobi, E. S. Hosseini, and M. R. Watts, "Large-scale nanophotonic phased array," *Nature*, vol. 493, no. 7431, pp. 195–199, Jan. 2013.
[11] H. Abediasl and H. Hashemi, "Monolithic optical phased-array transceiver in a standard SOI CMOS process," *Opt. Express*, vol. 23, no. 5, pp. 6509–6519, Mar. 2015.
[12] Y. Zhang, Y. C. Ling, K. Zhang, C. Gentry, D. Sadighi, G. Whaley, J. Colosimo, P. Suni, and S. J. B. Yoo, "Sub-wavelength-pitch silicon-photonic optical phased array for large field-of-regard coherent optical beam steering," *Opt. Express*, vol. 27, no. 3, pp. 1929–1940, Jan. 2019.
[13] N. Dupuis, A. V. Rylyakov, and C. L. Schow, D. M. Kuchta, C. W. Baks, J. S. Orcutt, D. M. Gill, W. M. J. Green, and B. G. Le, "Nanosecond-scale Mach–Zehnder-based CMOS photonic switch fabrics," *J. Lightw. Technol.*, vol. 35, no. 4, pp. 615–623, Feb. 18, 2017.
[14] W. Xie, T. Komljenovic, J. Huang, M. Tran, M. Davenport, A. Torres, P. Pintus, and J. E. Bowers, "Heterogeneous silicon photonics sensing for autonomous cars [Invited]," *Opt. Express*, vol. 27, no. 3, pp. 3642–3662, Feb. 2019.
[15] R.-L. Chao, Z. Ahmad, J. Chen, Y. Lai, and J.-W. Shi, "BJT-type optical phase shifter with small power consumption and fast response time on a silicon photonics foundry platform," *IEEE J. Sel. Topics Quantum Electron.*, vol. 26, no. 2, pp. 1–7, Mar. 2020.
[16] J. Zhou, J. Wang, L. Zhu, and Q. Zhang, "High baud rate all-silicon photonics carrier depletion modulators," *J. Lightw. Technol.*, vol. 38, no. 2, pp. 272–281, Jan. 15, 2020.
[17] A. Zanzi, C. Vagionas, A. Griol, A. Rosa, S. Lechago, M. Moralis-Pegios, K. Vyrsokinos, N. Pleros, J. Kraft, V. Sidorov, B. Sirbu, T. Tekin, P. Sanchis, and A. Brimont, "Alignment tolerant, low voltage, 0.23 V.cm, push-pull silicon photonic switches based on a vertical pn junction," *Opt. Express*, vol. 27, pp. 32409–32426, Oct. 2019.

RUI LIN CHAO was born in Taipei, Taiwan, in October 1991. He received the B.S. degree (Hons.) in nano science and engineering from National Chiao Tung University, Hsinchu, Taiwan, in 2014. He is currently pursuing the Ph.D. degree with the Department of Elecro-Optics, National Chiao Tung University, under the guidance of his advisor Prof. J. Chen, and co-advisor Prof. J. W. Shi, National Central University, focusing on slow light high speed silicon based modulators, high speed photodetectors, and high speed laser development and design.

ZOHAUDDIN AHMAD was born in Bihar, India, in 1989. He graduated from the Department of Nanoscience and Nanotechnology, Jamia Millia Islamia, New Delhi, India. He is currently pursuing the Ph.D. degree with the Department of Electrical Engineering, National Central University, Taiwan. His current research interests include high speed modulator-based lasers and silicon photonics.

JYEHONG (JASON) CHEN received the B.S. and M.S. degrees in electrical engineering from National Taiwan University, Taiwan, in 1988 and 1990, respectively, and the Ph.D. degree in electrical engineering and computer science from the University of Maryland, Baltimore, Baltimore, MD, USA, in 1998. He joined JDSU in 1998 as a Senior Engineer and holds 15 U.S. patents. He joined the Faculty of National Chiao Tung University, Taiwan, in 2003, where he is currently serving as a Professor and the Chairman of the Department of Photonics. He has published more than 100 articles in international journals and conferences and has been invited to give invited talks at numerous technical conferences, including OFC, Photonic West, and ECOC. His research interests are focused on hybrid access networks, long reach passive optical networks and optical interconnects.

YINCHIEH LAI received the B.S. degree in electrical engineering from National Taiwan University, Taipei, Taiwan, in 1985, and the M.S. and Ph.D. degrees in electrical engineering from the Massachusetts Institute of Technology, Cambridge, in 1989 and 1991, respectively. In 1991, he joined the Department of Photonics and the Institute of Electro-Optical Engineering, National Chiao Tung University, Hsinchu, Taiwan, where he is currently a Professor. He has been continuously working in the area of quantum optics, nonlinear optics, mode-locked fiber lasers, fiber devices, integrated optics, and optical communication.

JIN-WEI SHI (Senior Member, IEEE) was born in Kaohsiung, Taiwan, in January 1976. In 2003, he joined the Department of Electrical Engineering, National Central University, Taoyuan, Taiwan, where he has been served as a Professor, since 2011. In 2011 and 2012 and 2016 and2017, he joined the ECE Department, UCSB, as a Visiting Professor. He has authored or coauthored more than four book chapters, 140 Journal articles, 200 conference papers, and holds 30 patents. His current research interests include ultrahigh speed/power photodetectors, electro-absorption modulators, THz photonic transmitters, and VCSELs. In 2010, he was a recipient of the Da-You Wu Memorial Award.